ARTICLE

BIOTECHNOLOGY and BIOENGINEERING

Grafting of Antibacterial Polymers on Stainless Steel Via Surface-Initiated Atom Transfer Radical Polymerization for Inhibiting Biocorrosion by *Desulfovibrio desulfuricans*

S.J. Yuan,[1] F.J. Xu,[1,2] S.O. Pehkonen,[3] Y.P. Ting,[1] K.G. Neoh,[1] E.T. Kang[1]

[1]Department of Chemical and Biomolecular Engineering, National University of Singapore, 10 Kent Ridge Crescent, Singapore 119260, Singapore; telephone: +65-6516-2189; fax: +65-6779-1936; e-mail: cheket@nus.edu.sg

[2]College of Materials Science & Engineering, Beijing University of Chemical Technology, Beijing, P. R. China

[3]CEWIC, Thule Institute, University of Oulu, FI, Finland

Received 17 September 2008; revision received 16 November 2008; accepted 29 December 2008

Published online 6 January 2009 in Wiley InterScience (www.interscience.wiley.com). DOI 10.1002/bit.22252

ABSTRACT: To enhance the biocorrosion resistance of stainless steel (SS) and to impart its surface with bactericidal function for inhibiting bacterial adhesion and biofilm formation, well-defined functional polymer brushes were grafted via surface-initiated atom transfer radical polymerization (ATRP) from SS substrates. The trichlorosilane coupling agent, containing the alkyl halide ATRP initiator, was first immobilized on the hydroxylated SS (SS-OH) substrates for surface-initiated ATRP of (2-dimethylamino)ethyl methacrylate (DMAEMA). The tertiary amino groups of covalently immobilized DMAEMA polymer or P(DMAEMA), brushes on the SS substrates were quaternized with benzyl halide to produce the biocidal functionality. Alternatively, covalent coupling of viologen moieties to the tertiary amino groups of P(DMAEMA) brushes on the SS surface resulted in an increase in surface concentration of quaternary ammonium groups, accompanied by substantially enhanced antibacterial and anticorrosion capabilities against *Desulfovibrio desulfuricans* in anaerobic seawater, as revealed by antibacterial assay and electrochemical studies. With the inherent advantages of high corrosion resistance of SS, and the good antibacterial and anticorrosion capabilities of the viologen-quaternized P(DMAEMA) brushes, the functionalized SS is potentially useful in harsh seawater environments and for desalination plants.

Biotechnol. Bioeng. 2009;103: 268–281.

KEYWORDS: stainless steel; ATRP; DMAEMA; quaternization; biocorrosion

Introduction

Type 304 stainless steel (304 SS) exhibits excellent corrosion resistance in aquatic environments due to the formation of a thin, compact and chromium-enriched oxide film (Shibata and Okamoto, 1978). Nevertheless, 304 SS, as a low grade austenitic SS, is particularly susceptible to biocorrision of sulfate-reducing bacteria (SRB) and to localized corrosion by chloride and reducing sulfur compounds (Antony et al., 2007; Little and Wagner, 1993). The accelerated corrosion of SS by SRB is mainly caused by cathodic depolarization (Hamilton, 1985; Iverson, 1966), production of aggressive sulfide ions (Little et al., 2000), binding metal ions by extracellular polymeric substances (EPS) (Beech and Sunner, 2004), and formation of aggressive ferrous sulfide (Tributsch et al., 1998). Thus, biocorrosion is a great concern in aquatic environments and for maritime industries, as ~20–30% of corrosions are associated with biocorrosion at a direct cost of 30–50 billion dollars per year worldwide (Flemming, 1996). It is therefore of great importance to combat biocorrosion to prolong the service life of maritime structures and equipment.

Different strategies have been developed to address the growing need for combating biocorrosion (Akid et al., 2008; Al-Darbi et al., 2002; Cetin et al., 2007; Guezennec, 1994; Muthukumar et al., 2007; Sreekumari et al., 2005; Videla, 2002; Yebra et al., 2004). Biocidal treatment is a conventional approach for mitigating the problem of biofouling and biocorrosion in closed systems, such as potable water distribution systems (Mohanan et al., 2005; Videla, 2002). Alternatively, protective antifouling coatings, such as tributyltin (TBT)-based paints, are used extensively in seawater environments, despite concerns for their toxicity,

Correspondence to: E.T. Kang

Contract grant sponsor: National University of Singapore

Contract grant number: R-279-000-236-112

to combat biofouling and biocorrosion of metallic materials (Jelic-Mrcelic et al., 2006; Yebra et al., 2004). Although cathodic protection has been reported to effectively inhibit biocorrosion of SS by aerobic bacteria (Guezennec, 1994; Miyanaga et al., 2007), it has been found to have no effect on the adhesion of anaerobic bacteria, and is thus unable to prevent the initiation of pitting corrosion by SRB (de Mele et al., 1995). In view of environmental, ecological, and economical impacts, more recent efforts are focused on developing environmentally benign antimicrobial coatings to prevent bacterial adhesion and biofilm formation (Al-Darbi et al., 2002; Sreekumari et al., 2005; Telegdi et al., 2005), as the formation of biofilms is widely recognized as the key step in initiating biocorrosion. Different methods, such as, adsorption, sol-gel processing, and covalent binding, have been used for developing environmentally benign antimicrobial coatings on substrate surfaces to inactivate microorganisms during their initial attachment (Fu et al., 2005; Hu et al., 2005; Lee et al., 2004; Lin et al., 2003; Milović et al., 2005; Tiller et al., 2002; Xu et al., 2006). Tethering of polymer brushes on solid substrates via surface-initiated atom transfer radical polymerization (ATRP) is an effective method for modifying the surface properties of the substrate (Braunecker and Matyjaszewski, 2007). Well-defined and dense polymer brushes covalently bonded to a metal surface can render excellent mechanical and chemical protection to the substrate, alter the electrochemical characteristics of the interface, and provide versatility in coating formulation (Fan et al., 2005; Fu et al., 2005; Martin et al., 2007).

Accordingly, the purpose of this study is to provide an efficient, more permanent and environmentally friendly alternative to the functionalization of SS surface for biocorrosion protection. Coupling of an alkyl halide-containing silane on the hydroxylated SS surface provides not only a dense passivation layer, but also initiation sites for tethering bactericidal poly(2-dimethyamino)ethyl methacrylate) P(DMAEMA) brushes via surface-initiated ATRP. The process is shown schematically in Figure 1. The incorporation of viologen moieties in the grafted polymer coatings is designed to further enhance the antibacterial and anticorrosion capabilities of the quaternized P(DMAEMA) brushes, based on the fact that not only have the polymers containing quaternary ammonium groups been shown to be lethal on contact with both gram-negative and gram-positive bacteria (Hu et al., 2005; Lee et al., 2004), they are also effective in inhibiting corrosion of metals in aggressive environments (Popova et al., 2007).

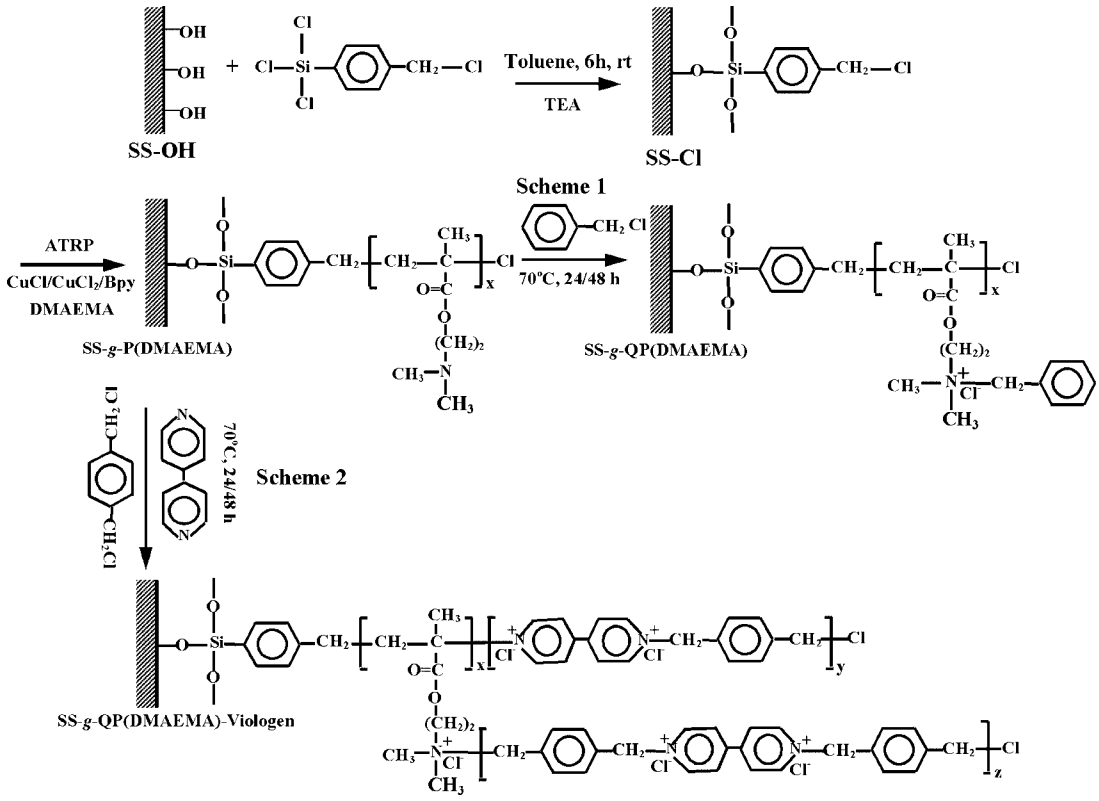

Figure 1. Schematic diagram illustrating the process of coupling of CTS to SS-OH surface (the SS-Cl surface), surface-initiated ATRP of DMAEMA from the SS-Cl surface (the SS-*g*-P(DMAEMA) surface), and subsequent functionalization, via quaternization, of the SS-*g*-P(DMAEMA) surfaces into antibacterial SS-*g*-QP(DMAEMA) and SS-*g*-QP(DMAEMA)-Viologen surfaces.

Materials and Methods

Materials

Type 304 SS (nominal composition: Fe 71.376%, Ni 8.18%, C 0.053%, Cr 18.08%, Cu 0.06%, Mn 1.68%, Mo 0.05%, N 0.047%, P 0.037%, S 0.007%, and Si 0.43%) was purchased from Metal Samples Co. (Munford, AL). (2-Dimethyamino)-ethyl methacrylate) (DMAEMA, >99%), 4-(chloromethyl)-phenyl trichlorosilane (CTS, 97%), 2,2′-bipyridine (Bpy), copper(I) chloride (99%), copper(II) chloride (97%), benzyl chloride (99%), dichloro-*para*-xylene, and 4,4′-dipyridine (98%) were obtained from Sigma–Aldrich Chemical Co. (St. Louis, MO). Solvents, such as chloroform, acetone, toluene (99.8%), and *N*,*N*′-dimethylformamide (DMF, 99.8%), triethanolamine (TEA), and other chemicals were of reagent grade and were used as received. Yeast extract and agar were purchased from Oxoid Ltd. (Hampshire, UK). The sulfate-reducing bacterium of *Desulfovibrio desulfuricans* was obtained from American Type Culture Collection (ATCC, No. 27774). Phosphate buffer solutions (PBS) (containing NaH_2PO_4 of 4.68 g/L and Na_2HPO_4 of 8.662 g/L) was freshly prepared and sterilized in an autoclave before use.

Immobilization of the Initiator on the Hydroxylated Coupon (SS-OH) Surfaces

The 3 mm thick SS plates were polished sequentially up to 1,200 grit SiC paper and cut into coupons of about 10 mm × 10 mm in area. The newly polished coupons were washed with copious amounts of deionized water, acetone, ethanol, and deionized water, in that order, for 5 min each to degrease and clean the surface. The grease-free and smooth coupons were treated by *Piranha* solution to generate a hydroxyl-enriched (SS-OH), or a hydroxylated surface. Details on the preparation and characterization of the hydroxylated surface had been described previously (Martin et al., 2007; Yuan et al., 2008). The silane coupling agent, CTS, was immobilized on the hydroxylated substrate via self-assembly. The hydroxylated coupons were immersed in 20 mL of anhydrous toluene solution, containing 0.5 mL of TEA and 0.1 mL of CTS, for 6 h at room temperature. After the reaction, the coupons were isolated and ultrasonically washed with copious amounts of chloroform, acetone, methanol, and finally, deionized water, in that order. The silane-coupled substrates (SS-Cl), containing the alkyl halide ATRP initiator, were then stored in a vacuum desiccator after being dried under reduced pressure.

Surface-Initiated ATRP of DMAEMA

For the preparation of DMAEMA polymer (P(DMAEMA)) brushes on the SS-Cl surface, DMAEMA (4 mL, 23.7 mmol), CuCl (23.7 mg, 0.237 mmol), $CuCl_2$ (6.4 mg, 0.048 mmol), and Bpy ligand (35.8 mg, 0.237 mmol) were added to 4 mL of methanol in a Pyrex® tube. The SS-Cl substrate was introduced into the reaction mixture after it was stirred and degassed with argon for 30 min. The reaction tube was sealed and kept in a 35°C water bath for 6 and 24 h to produce the respective SS-*g*-P(DMAEMA)$_1$ and SS-*g*-P(DMAEMA)$_2$ surfaces. After the reaction, the P(DMAEMA) brushes were washed sequentially with copious amounts of deionized water and methanol to ensure the complete removal of the physically adsorbed polymers, if any.

Quaternization of the SS-g-P(DMAEMA) Surfaces

As shown in Figure 1, two different schemes were chosen to prepare the bactericidal surfaces based on the SS-g-P(DMAEMA)$_2$ surfaces. In Scheme 1, the P(DMAEMA) brushes were directly converted, via *N*-alkylation reaction with benzyl chloride, to the polycationic chains with quaternary ammonium groups. The coupons were immersed in 10 mL of 0.12 M DMF solution of benzyl chloride in a Pyrex® tube at 70°C for 24 and 48 h to produce the SS-*g*-QP(DMAEMA) surfaces. In Scheme 2, the P(DMAEMA) brushes were quaternized by dichloro-*para*-xylene together with viologen moieties, via reaction of the SS-g-P(DMAEMA)$_2$ surfaces with an equimolar (0.12 M) mixture of dichloro-*para*-xylene and 4,4′-dipyridine in 10 mL of DMF at 70°C for 24 and 48 h, respectively, to generate the SS-g-P(DMAEMA)-Viologen hybrids (Monk, 1998; Zhao et al., 2002). The coupons were sequentially washed with large amounts of DMF, acetone, and deionized water to remove the unreacted reactants.

Surface Characterization

The surface composition of the functionalized substrates was determined by X-ray photoelectron spectroscopy (XPS). The XPS measurement was performed on a Kratos AXIS HSi XPS spectrometer with an Al Kα X-ray source (1486.6 eV photons), using procedures as described previously (Yuan et al., 2007). Static water contact angles of the pristine (hydroxylated) and surface-functionalized coupons were measured at 25°C and 60% relative humidity, using the sessile drop method with a 3 μL water droplet, in a telescopic goniometer (Rame-Hart model 100-00-(230), Rame-Hart, Inc., Mountain Lake, NJ). The telescope with a magnification power of 23× was equipped with a protractor of 1° graduation. The contact angles reported were the mean value from four substrates, with the value of each substrate obtained by averaging the contact angles from three surface locations.

Microorganism Cultivation and Inoculation

Gram-negative *D. desulfuricans* (ATCC, No. 27774) bacterium was cultured in the simulated seawater-based

modified Baar's (SSMB) medium, as those described in detail previously (Yuan et al., 2008). Each liter of the SSMB medium contained 23.476 g of NaCl, 3.917 g of Na_2SO_4, 0.192 g of $NaHCO_3$, 0.664 g of KCl, 0.096 g of KBr, 10.61 g of $MgCl_2 \cdot 6H_2O$, 1.469 g of $CaCl_2 \cdot 6H_2O$, 0.026 g of H_3BO_3, 0.04 g of $SrCl_2 \cdot 6H_2O$, 0.41 g of $MgSO_4 \cdot 7H_2O$, 0.1 g of NH_4Cl, 0.1 g of $CaSO_4$, 0.05 g of K_2HPO_4, 0.1 g of $(NH_4)_2Fe(SO_4)_2$, 0.5 g of tri-sodium citrate, 3.5 g of sodium lactate, and 1.0 g of yeast extract. The medium was adjusted to 7.5 ± 0.1 in pH value using a 5 M NaOH solution, and then sterilized by autoclaving at 121°C for 20 min at 1 bar.

For the inoculation medium, a 1 mL aliquot of the 3-day-old *D. desulfuricans* culture was introduced into 500 mL of the SSMB medium in a Scottch Duran bottle (1.0 L). The medium was incubated at 30°C in an anaerobic workstation (Don Whitley, Model MASC MG 500, Maharashtra, India), and maintained in an atmosphere containing 5% H_2, 5% CO_2, and 90% N_2. The bacterial cell counts were determined using the 3-tube most probable number (MPN) method. The pristine and surface-functionalized coupons were first sterilized in 70% ethanol solution for 8 h and dried by purging with pure N_2. When the bacterial density of *D. desulfuricans* had increased to more than 10^6 MPN mL^{-1} after 2 days of incubation, these coupons were aseptically introduced into the *D. desulfuricans* inoculated SSMB medium to determine their antibacterial and anticorrosion properties. The planktonic viable cell density of *D. desulfuricans* in the bulk medium remained in the range of 10^5–10^8 MPN mL^{-1}, with the biogenic sulfide ions in a range of 30 and 40 mg L^{-1} (about 0.94–1.25 mM), throughout the exposure periods in the present study, as those reported previously (Yuan et al., 2008).

Adhesion and Viability Assay of the Surface-Functionalized Coupons

The ability of the surface-functionalized coupons in inhibiting bacterial adhesion was revealed by scanning electron microscopy (SEM) images. The sample fixation and preparation for SEM imaging were as follows. The coupons were first washed with PBS to remove the adsorbed nutrients of yeast extract as well as the dead bacterial cells on the outermost surface at the end of predetermined exposure period. The coupons were then immersed in 3 vol% glutaradehyde (GA) of PBS for 5 h at −4°C. After that, the substrates were washed with PBS, followed by step dehydration with 25%, 50%, 70%, 95%, and 100% ethanol for 5 min each. The coupons were then dried and sputter-coated with a thin film of platinum for SEM imaging purpose. To observe the surface corrosion damage, the bacterial cells and the corrosion products were removed from the coupon surface with sterilized cotton swabs immediately after the coupons were removed from the medium, followed by rinsing thrice with sterilized deionized water and drying with a stream of pure N_2. For comparison purpose, SEM images of the pristine coupons after various exposure periods in the SSMB culture medium were obtained to ascertain the effect of *D. desulfuricans* on SS substrates. For SEM imaging, four areas on the coupon surface were randomly chosen to be representative of the entire coupon surface.

To assess the bactericidal properties of the surface-functionalized coupon in a more quantitatively manner, the number of viable cells on each substrate surface was enumerated as a function of exposure time. The viable cells attached to the pristine and the surface-functionalized coupons were estimated by the 3-tube MPN method. The procedures were as follows. After the prescribed exposure time, the coupons were gently removed from the inoculated SSMB medium, and introduced immediately into 10 mL of sterile PBS, followed by sonication in an ultrasonic bath (Cole-Parmer, Vernon Hills, IL) for 3 min at a frequency of 40–50 KHz. Decimal serial dilutions with PBS were repeated with each initial bacterial suspension. One milliliter of each diluted suspension was inoculated in triplicate in separate tubes containing 9 mL of the culture medium. After 72 h of incubation at 30°C, the broth from each tube was examined for the presence or the absence of bacterial growth. The results after multiplication with the dilution factor were expressed as mean viable cell counts for each substrate.

Evaluation of Anticorrosion Properties of the Surface-Functionalized Coupons

To assess the anticorrosion properties of the surface-functionalized coupons, Tafel plots, impedance spectra, and cyclic polarization curves were obtained on an Autolab PGSTAT 30 electrochemical work station (Ecochemie Co., Utrecht, the Netherlands). A conventional glass corrosion cell with a capacity of 500 mL was used. The pristine and the surface-functionalized coupons were mounted in a PVDF holder, leaving a circular area of 0.785 cm^2, to serve as the working electrode. An Ag/AgCl electrode was used as the reference electrode, and a platinum rod as the counter electrode. After the predetermined exposure time in the *D. desulfuricans* inoculated SSMB medium, electrochemical measurements similar to those described previously were performed (Yuan et al., 2008). The inhibition efficiency (IE) of the grafted polymer coatings on the surface functionalized coupons can be calculated from the following equation (Yuan et al., 2007):

$$\mathrm{IE}\% = \frac{i_0 - i_{\mathrm{corr}}}{i_0} \tag{1}$$

wherein, i_o and i_{corr} are the corrosion current densities of the pristine and the surface-functionalized coupons, respectively, as determined from the analysis of Tafel plots. In comparison, electrochemical measurements were also carried out on the pristine coupons in the sterile SSMB medium under the same conditions.

Results and Discussion

Grafting of Antibacterial Polymers From Stainless Steel Via Surface-Initiated ATRP

The surface composition of SS coupons at different stages of surface modification was characterized by XPS. The wide scan spectrum of the oxidized/hydroxylated (SS-OH) surface, from the *piranha* solution treatment (Martin et al., 2007; Yuan et al., 2008), is dominated by Fe 2p, Cr 2p, O 1s and C 1s signals (Fig. 2a). The presence of two dominant peak components in the O 1s core-level spectrum at the binding energies (BEs) of 529.9 and 531.7 eV, attributable to oxide and hydroxide species (Fig. 2b), respectively (Wagner et al., 1992), is consistent with the formation of a thin oxide/hydroxide film on the coupon surface. The SS-OH surface has a static water contact angle of about 18° (Table I).

For grafting of polymer brushes from the metal substrate via surface-initiated ATRP, a uniform layer of initiators immobilized on the substrate is indispensable (Braunecker and Matyjaszewski, 2007). Figure 2c–f show the respective wide scan spectrum, Cl 2p, Si 2p, and C 1s core-level spectra of the 4-(chloromethyl)phenyl trichlorosilane (CTS)-coupled surface (SS-Cl surface). Four additional photoelectron lines at BEs of about 99, 151, 197, and 230 eV, attributable to the Si 2p, Si 2s, Cl 2p, and Cl 2s species, respectively, have appeared in the wide scan spectrum (Fig. 2c), as compared to that of the hydroxylated surface (Fig. 2a). The [Si]/[C]/[Cl] ratio, as determined from the Si 2p, C 1s, and Cl 2p core-level spectral area, is about 1.0:7.1:1.1, which is comparable to that of the theoretical value of 1:7:1 for CTS. The curve-fitted C 1s core-level spectrum has three peak components with BEs at 283.9, 284.6, and 286.2 eV, attributable to the C–Si, C–C/C–H, and C–Cl species (Hu et al., 2006), respectively (Fig. 2f). The area ratio of the three peak components is 1.0:5.0:1.1, which is in good agreement with the theoretical ratio of 1:5:1 for CTS. The π–π^* shake-up satellite associated with the aromatic ring of CTS is also discernible at the BE of about 291 eV. The increase in static water contact angle from about 18° to 92° (Table I) is also indicative of the successful immobilization of CTS on the SS-OH surface. The Cl $2p_{3/2}$ and Cl $2p_{1/2}$ spin-orbit split doublet at the BEs of about 200 and 201.6 eV is attributed to the covalently bonded chlorine (Wagner et al., 1992) of the benzyl chloride moiety of the immobilized silane (Fig. 2d). Thus, the benzyl chloride groups have been successfully immobilized on the SS-OH surface to cater for the subsequent ATRP process from the SS-Cl surface.

In this work, the molar ratio of [DMAEAM (monomer)]/[CuCl (catalyst)]/[$CuCl_2$ (deactivator)]/[Bpy (ligand)] was controlled at 100:1:0.2:1 to produce the P(DMAEMA)-grafted SS surfaces, or the SS-*g*-P(DMAEMA) surfaces. The SS-*g*-P(DMAEMA) surface becomes more hydrophilic, as its contact angle decreases from about 92° to about 56°, and about 53°, respectively, after 6 and 24 h of ATRP (Table I). Figure 3a–d shows the C 1s, N 1s, and Cl 2p core-level

Table I. Static water contact angles of different substrate surfaces.

Sample surface	Static water contact angles (mean ± SD, degree)
Pristine[a]	47 ± 3
SS-OH[b]	18 ± 2
SS-Cl[c]	92 ± 4
SS-*g*-P(DMAEMA)$_1$[d]	56 ± 3
SS-*g*-P(DMAEMA)$_2$[e]	53 ± 4
SS-*g*-QP(DMAEMA)[f]	37 ± 2
SS-*g*-QP(DMAEMA)-Vilogen[g]	24 ± 1

SD, standard deviation.
[a]Pristine refers to a newly polished stainless steel (SS) coupon.
[b]SS-OH was obtained after the newly polished SS coupon was treated in the *piranha* solution for 30 min.
[c]SS-Cl corresponds to the SS-OH surface with immobilized CTS.
[d]Reaction conditions: [DMAEMA]/[CuCl]/[$CuCl_2$]/[bpy] = 100:1:0.2:2 in methanol/DMAEMA (1:1, v/v) at 35°C for 6 h.
[e]Reaction conditions: [DMAEMA]/[CuCl]/[$CuCl_2$]/[bpy] = 100:1:0.2:2 in methanol/DMAEMA (1:1, v/v) at 35°C for 24 h.
[f]SS-*g*-QP(DMAEMA) refers to the SS-*g*-P(DMAEMA)$_2$ surface quaternized with benzyl chloride for 48 h.
[g]Reaction conditions: [dichloro-*para*-xylene]/[4,4′-dipyridine] = 1:1 in DMF at 70°C for 48 h.

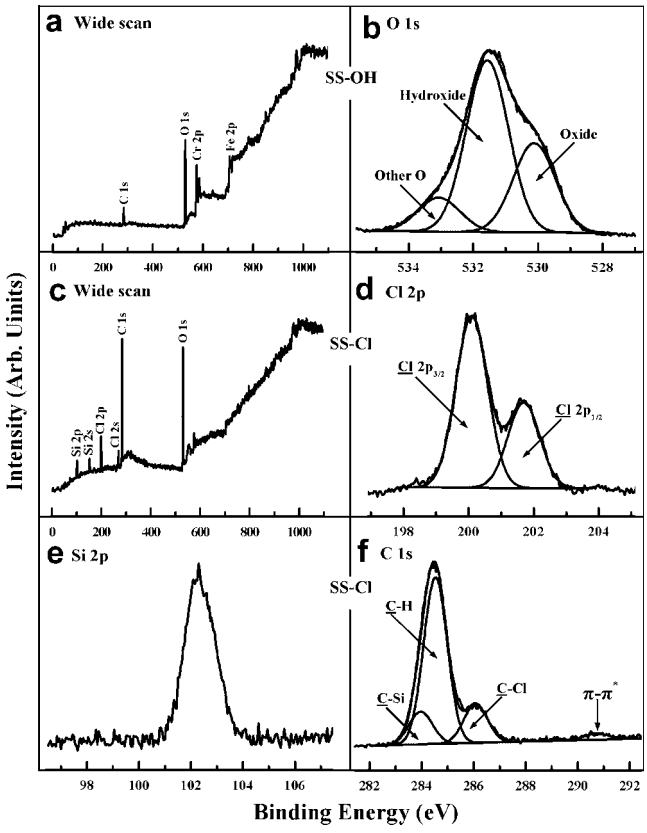

Figure 2. **a**,**b**: Wide scan and O 1s core-level spectra of the SS-OH surface, and (**c**–**f**) wide scan, Cl 2p, Si 2p, and C 1s core-level spectra of the SS-Cl surface (the reaction conditions are given in Table I).

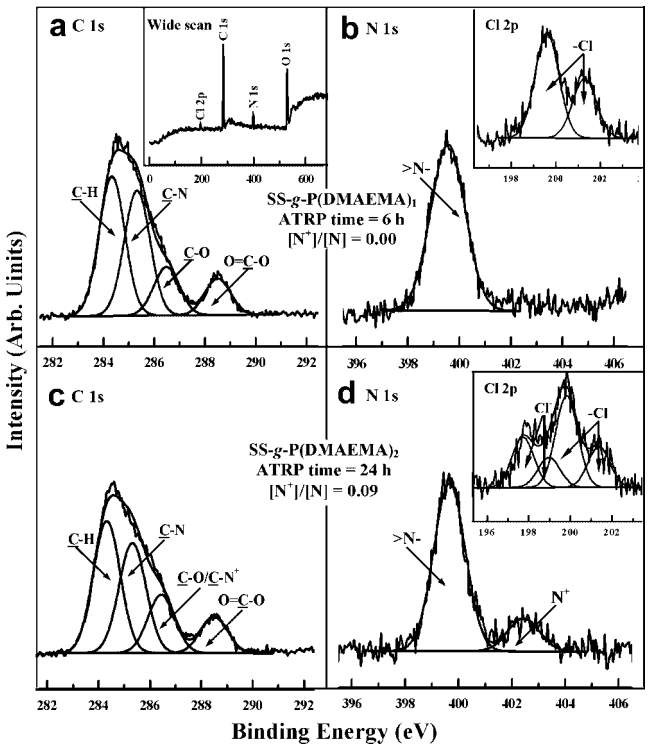

Figure 3. Wide scan, C 1s, N 1s, and Cl 2p core-level spectra of the (**a**,**b**) SS-*g*-P(DMAEMA)$_1$ surface, and (**c**,**d**) SS-*g*-P(DMAEMA)$_2$ surface (the reaction conditions are given in Table I).

spectra of the respective SS-*g*-P(DMAEMA)$_1$ and SS-*g*-P(DMAEMA)$_2$ surfaces from 6 and 24 h of ATRP, respectively. The disappearance of the Si signals and the appearance of N signals in the wide scan spectrum of the SS-*g*-P(DMAEMA)$_1$ surface indicates that the thickness of the P(DMAEMA) brushes is larger than the probing depth of the XPS technique (about 8 nm in an organic matrix (Wagner et al., 1992)) after 6 h of ATRP time (inset of Fig. 3a). The [N]/[C] ratio, as determined from the sensitivity-factor-corrected N 1s and C 1s core-level spectral area ratio, is around 0.12, which is close to the theoretical [N]/[C] ratio of 0.125 for DMAEMA. The C 1s core-level spectrum of the SS-*g*-P(DMAEMA)$_1$ surface can be curve-fitted into four peak components with BEs at 284.6, 285.5, 286.2, and 288.5 eV, attributable to the C–H, C–N, C–O, and O=C–O species (Wagner et al., 1992), respectively (Fig. 3a). The area ratio of [C–H]/[C–N]/[C–O]/[O=C–O] (about 3.3:2.8:1.1:1.0) is consistent with the chemical structure of P(DMAEMA) (theoretical component ratio of 3:3:1:1). The N 1s core-level spectrum of the SS-*g*-P(DMAEMA)$_1$ surface shows a predominant peak component at the BE of 399.4 eV, attributable to the neutral amine species (Fig. 3b) (Xu et al., 2006). The persistence of Cl species (Cl $2p_{3/2}$ and Cl $2p_{1/2}$ doublet, inset of Fig. 3b) is consistent with the fact that the "living" chain end from the ATRP process involves a dormant alkyl halide group, which can be re-activated to initiate the subsequent block copolymerization.

Upon prolonging the ATRP time to 24 h, the N 1s core-level spectrum of the SS-*g*-P(DMAEMA)$_2$ surface show an additional minor peak component at the BE of about 402.6 eV, attributable to the positively charged nitrogen (N^+) species (Xu et al., 2006) (Fig. 3d), indicating that the extended ATRP time has resulted in a small degree (about 9%) of quaternaization of the longer P(DMAEMA) chains by the dormant alkyl halide groups at the chain ends from the ATRP process (Liu et al., 1999; Wang and Matyjaszewski, 1995). The self-quaternization effect is further confirmed by the appearance of an anionic chloride species (Cl^-, with a Cl $2p_{3/2}$ BE at about 197 eV (Hu et al., 2005)) in the Cl 2p core-level spectrum (inset of Fig. 3d). The deviation in peak component area ratio in the curve-fitted C 1s core-level spectrum of Figure 3c from that of Figure 3a is consistent with the partial quaternization of the P(DMAEAM) chains. The surface-initiated ATRP is strongly dependant on the reaction time, and the thickness of the grafted polymeric brushes increases linearly with the polymerization time (Liu et al., 1999). Thus, the SS-*g*-P(DMAEMA)$_2$ surface with a thicker polymer layer is used in the subsequent *N*-alkylation reaction to produce the antimicrobial surface.

The pendant tertiary amino groups of P(DMAEMA) can be quaternized, based on the two proposed schemes in Figure 1, to produce the biocidal effect. In Scheme 1, the SS-*g*-P(DMAEMA)$_2$ surface is quaternized directly by benzyl chloride to produce the quaternary ammonium groups in the polycationic chains (the SS-*g*-QP(DMAEMA) surface). Parts a–d of Figure 4 show the respective N 1s and Cl 2p core-level spectra of the SS-*g*-QP(DMAEMA) surface after 24 and 48 h of the quaternization reaction. The N 1s core-level spectra can be curve-fitted into two peak components with BEs at about 399.4 and 402.6 eV, attributable to the neutral amine and positively charged nitrogen (N^+) species, respectively (Fig. 4b and d). The $[N^+]/[N_T]$ ratios are about 0.31 and 0.36, respectively, after the reaction time of 24 and 48 h, indicating that about one out of three DMAEMA repeat units have been quaternized. Prolonging the time of quaternization reaction does not seem to result in a higher extent of quaternization. The corresponding Cl 2p core-level spectra are curve-fitted into two spin-orbit-split doublets with BEs for the Cl $2p_{3/2}$ peak components at about 197 and 200 eV (Fig. 4a and c), attributable to the ionic chloride (Cl^-) and covalent chlorine (–Cl) species, respectively (Hu et al., 2005). The covalent chloride species is probably associated with the chloride end groups, preserved throughout the ATRP reaction. The static water contact angle decreases from about 53° to 37° after 48 h of quaternization reaction (Table I).

In Scheme 2, the reaction of the Si-*g*-P(DMAEMA)$_2$ surface with 4,4′-dipyridine and dichloro-*para*-xylene results in the formation of surface-coupled viologen, or the SS-*g*-QP(DMAEMA)-Viologen surfaces. The respective Cl 2p and N 1s core-level spectra of the SS-*g*-

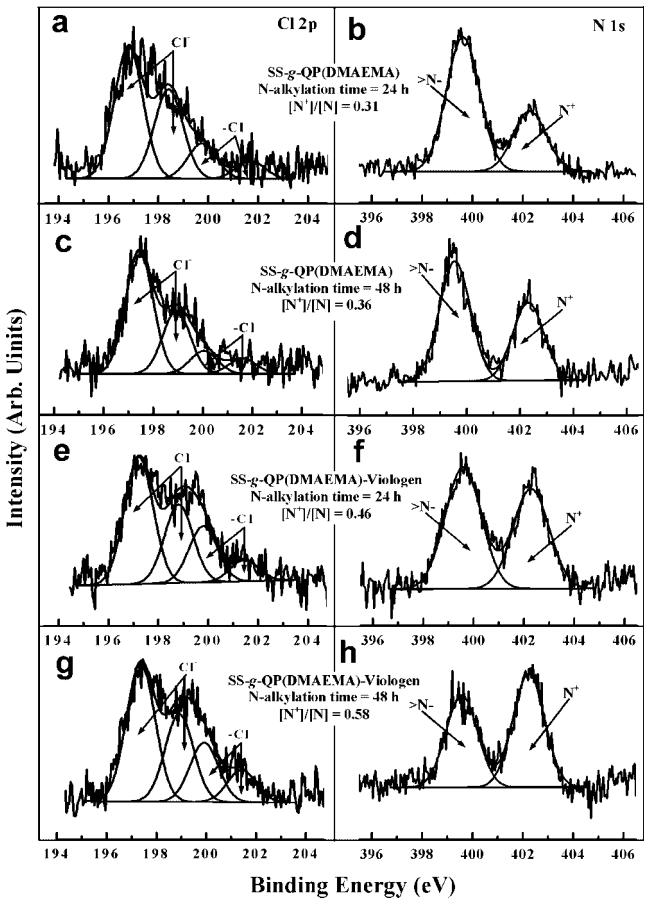

Figure 4. Cl 2p and N 1s core-level spectra of the (**a**–**d**) SS-*g*-QP(DMAEMA) surface, and (**e**–**h**) SS-*g*-QP(DMAEMA)-Viologen surface from 24 and 48 h of quaternization reaction of the SS-*g*-P(DMAEMA)$_2$ surface (the reaction conditions are given in Table I).

QP(DMAEMA)-Viologen surfaces after 24 and 48 h of quaternization reaction are shown in Figure 4e–h. The $[N^+]/[N_T]$ ratios are about 0.46 and 0.58, respectively, after 24 and 48 h of reaction (Fig. 4f and h). The surface concentration of positively charged nitrogen (N^+) species increases substantially upon prolonging the quaterization time. These results suggest: (i) the successful coupling of viologen to the polycationic chains, and (ii) an increase in the conversion of the neutral amine species of the P(DMAEMA) chains to N^+ species. It has been reported that the thickness of the viologen layers on the P(DMAEMA)-grafted Si wafer surface is about 2–3 nm after 24 h of quaternization reaction at 70°C (Zhao et al., 2002). The Cl 2p core-level spectra (Fig. 4e and g) of the SS-*g*-QP(DMAEMA)-Viologen surfaces also consist of the ionic chloride (Cl^-) and covalent chlorine (–Cl) species. The SS-*g*-QP(DMAEMA)-Viologen surface becomes more hydrophilic, as its static water contact angle has decreased to 24° (Table I). The SS-*g*-QP(DMAEMA) and the SS-*g*-QP(DMAEMA)-Viologen coupons from 48 h of quaternization reaction are subsequently used for evaluating the antibacterial and anticorrosion properties of the grafted polymer-viologen coating.

Adhesion and Viability Assay of the Surface-Functionalized Coupons

Figure 5 shows the representative SEM images of the pristine (newly polished) coupons after various exposure periods in the sterile and the *D. desulfuricans*-inoculated SSMB medium. A newly polished SS coupon before exposure shows a uniform and smooth surface (Fig. 5a). The surfaces

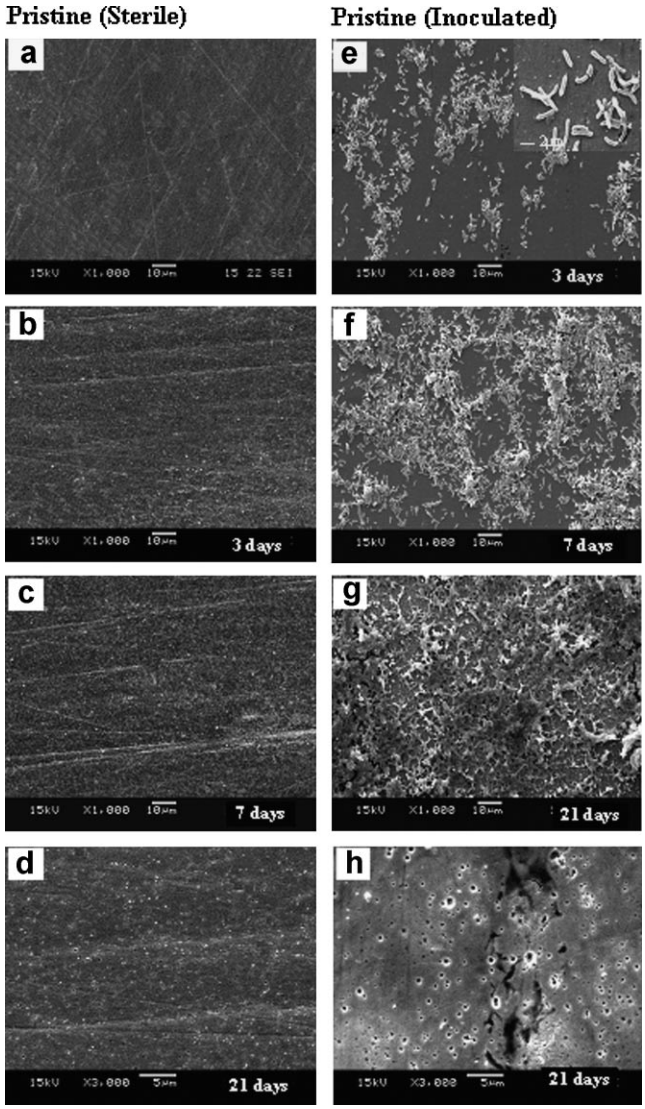

Figure 5. **a**: SEM image (a) represents of a newly polished coupon before exposure. SEM images of (**b**–**d**) the pristine coupons after 3, 7, and 21 days of exposure in the sterile SSMB medium, and (**e**–**g**) the pristine coupons after 3, 7, and 21 days of exposure in the *D. desulfuricans* inoculated SSMB medium. **h**: SEM images (3,000×) captured upon removal of the corrosion products and bacterial cells.

of pristine coupons remain almost unchanged after various exposure periods in the sterile medium, as shown in Figure 5b–d, and no pitting corrosion is observed. This result is in good agreement with the negative hysteresis in the cyclic polarization curves of the pristine SS coupon after 21 days of exposure in the sterile SSMB medium (Fig. 6a) (Tait, 1978). Numerous bacterial cells, either individually or in small clusters, are observed on the pristine SS coupon after 3 days of exposure in the inoculated SSMB medium. The bacterial cells are rod-shaped, with a length of above 4 μm (inset of Fig. 5e). Active cell growth, as well as cell division, is also observed (Fig. 5e). Upon prolonging the exposure time to 7 days, the bacterial micro-colonies become dense, and aggregate to form patchy biofilms (Fig. 5f). Dense and lumpy deposits are observed on the pristine SS coupons after 21 days of exposure (Fig. 5g). Bacterial cells are visible among the corrosion products. It has been reported that the discontinuity in the surface film favors localized attack by aggressive ions, such as Cl^- and S^{2-}, leading to the initiation of pitting or crevice corrosion (Moreno et al., 1991). As a result, extensive micropits and crevice are present on the pristine SS coupons upon removal of the corrosion deposits (Fig. 5h). The observation is consistent with the positive hysteresis in the cyclic polarization curve of the pristine SS coupons in the inoculated SSMB medium (Fig. 6b) (Tait, 1979). These results further indicate that sulfide-producing bacteria are detrimental to the passivity of SS (Jack et al., 1992; Moreno et al., 1991).

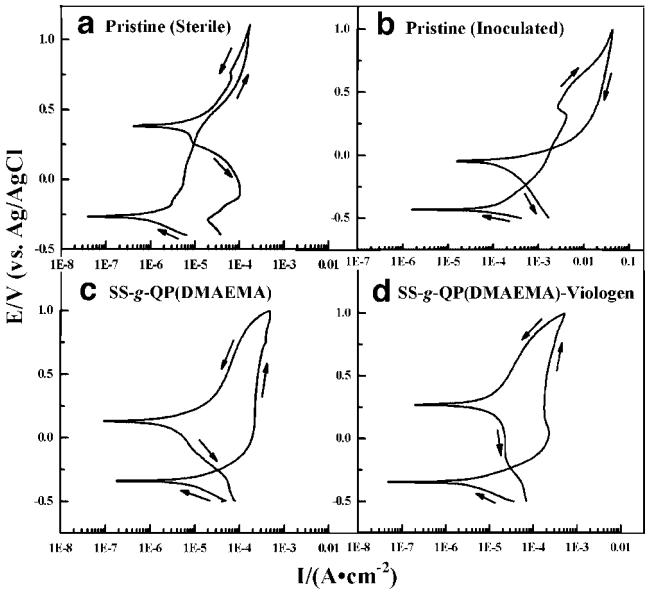

Figure 6. Cyclic polarization curves of (**a**) the pristine coupon after 21 days of exposure in the sterile SSMB medium, and (**b**) the pristine, (**c**) the SS-*g*-QP(DMAEMA) and (**d**) the SS-*g*-QP(DMAEMA)-Viologen coupons after 21 days of exposure in the *D. desulfuricans* inoculated SSMB medium.

Figure 7 shows the representative SEM images of the SS-*g*-QP(DMAEMA) and the SS-*g*-QP(DMAEMA)-Viologen surfaces after various exposure periods in the *D. desulfuricans* inoculated medium. It is obvious that inhibition of bacterial adhesion is correlated with the concentration of positively charged nitrogen (N^+) species on the coupon surface. As shown in Figure 7a–c, the number of bacterial cells adhered to the SS-*g*-QP(DMAEMA) surfaces are significantly reduced. The bacterial cells are sparsely distributed as single cells, with an oval or cylindrical shape of around 2 μm or less in length (inset of Fig. 7a). The deformation in bacterial shape and the reduction in bacterial length suggest that the surface-bearing polycationic N^+ species not only can inhibit the attachment of anaerobic *D. desulfuricans*, but also exhibit bactericidal

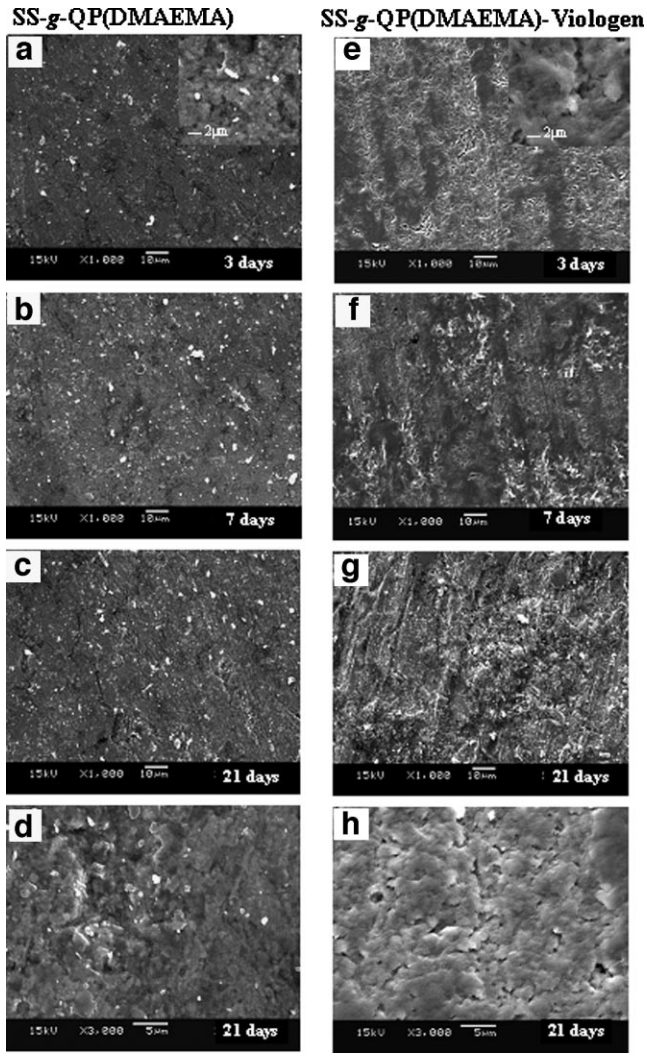

Figure 7. SEM images of (**a–d**) the SS-*g*-QP(DMAEMA) and (**e–h**) the SS-*g*-QP(DMAEMA)-Viologen surfaces after 3, 7, and 21 days of exposure in the *D. desulfuricans* inoculated medium. d,h: SEM images (3,000×) captured upon the removal of the corrosion products and bacterial cells.

effects (Tiller et al., 2001). The relative concentration of surface N^+ species has increased significantly on the SS-*g*-QP(DMAEMA)-Viologen surface, as compared to that of the SS-*g*-QP(DMAEMA) surface, with almost two-thirds of the nitrogen atoms existing as the N^+ species. As a result, bacterial adhesion to this surface is almost completely inhibited throughout the exposure periods (Fig. 7e–g). It has been reported that the quaternary ammonium groups can disrupt the plasmic membrane of the bacteria to cause the release of intracellular materials (Lin et al., 2003; Milović et al., 2005). Viologens are the pyridinium-type polymers with the polycationic groups and possess effective anti-bacterial properties (Monk, 1998). The high inhibitive property of the SS-*g*-QP(DMAEMA)-Viologen surface can thus be attributed to the combined effect of the quaternary ammonium groups on the main chain of the P(DMAEMA) and the surface-coupled viologen moieties. Figure 7d and h show the surface morphology, after removal of the corrosion products and bacterial cells, of the respective SS-QP(DMAEMA) and the SS-QP(DMAEMA)-Viologen surfaces after 21 days of exposure in the inoculated medium. No damage of the grafted polymer coating is observed. The negative hysteresis in the cyclic polarization curves further confirm that no localized corrosion occurs under the grafted polymer coatings (Fig. 6c and d).

The bactericidal effect of the surface-functionalized coupons are also found to be correlated with the surface concentration of positively charged nitrogen (N^+) species on the substrate surfaces, as revealed by the number of viable bacterial cells adhered on the substrate surface. Viable cell counts on the various substrate surfaces as a function of exposure time were performed and compared in Figure 8. The viable cell counts on the pristine SS coupon surface were $>10^5$ cells/cm^2 after 3 day of exposure, and increased rapidly by more than two orders of magnitude after 7 days of exposure. Whereas, the SS-*g*-QP(DMAEMA) surface showed the desired biocidal effect, as the number of viable cells was $<10^3$ cells/cm^2 throughout the exposure period. Arising from a higher surface concentration of the N^+ species, the SS-*g*-QP(DMAEMA)-Viologen

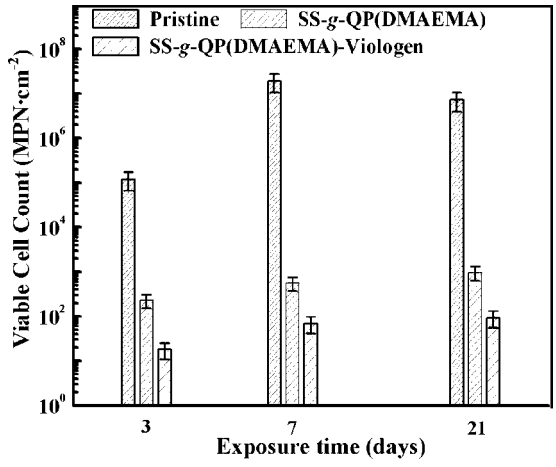

Figure 8. The number of viable *D. desulfuricans* cells adhered on the pristine, the SS-*g*-QP(DMAEMA) and the SS-*g*-QP(DMAEMA)-Viologen surfaces as a function of exposure time in the *D. desulfuricans* inoculated SSMB medium.

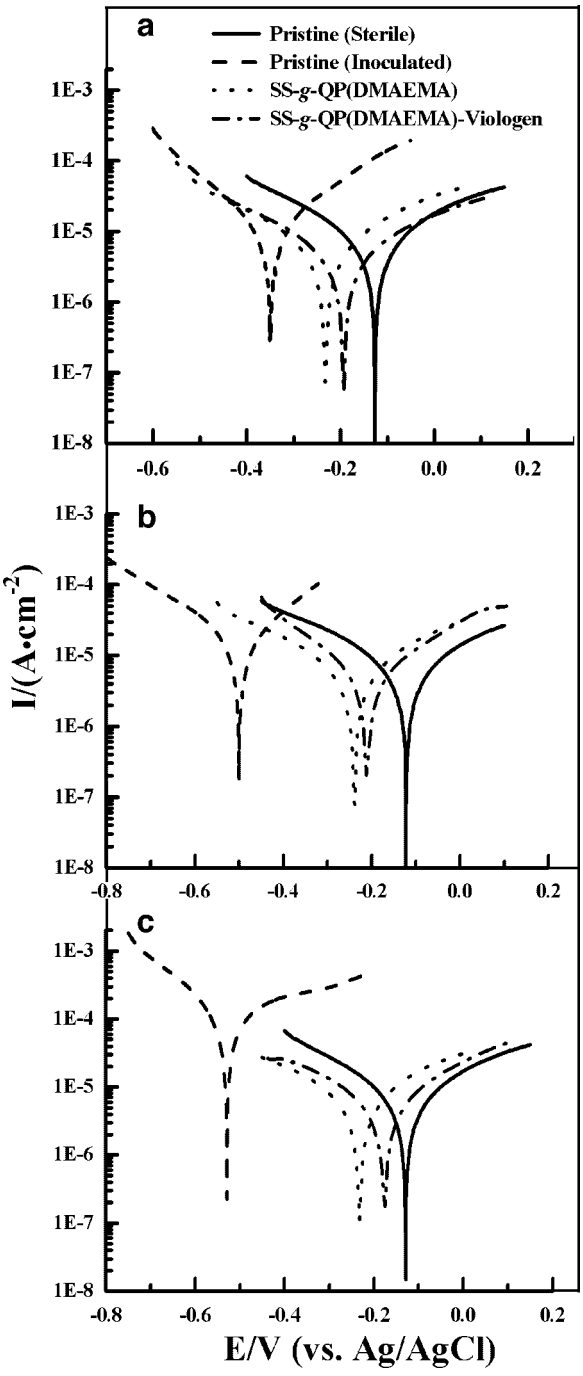

Figure 9. Tafel plots of the pristine, SS-*g*-QP(DMAEMA) and SS-*g*-QP(DMAEMA)-Viologen coupons in the *D. desulfuricans* inoculated SSMB medium, as well as the pristine coupons in the sterile SSMB medium for (**a**) 3, (**b**) 7, and (**c**) 21 days.

surface exhibited an even higher antibacterial efficiency. Bacterial adhesion and proliferation were further inhibited, with the viable cell counts on the surface decreasing to $<10^2$ cells/cm^2.

Anticorrosion Behavior of the Surface-Functionalized Coupons

Figure 9a–c shows Tafel plots of the pristine (newly polished) and the surface-functionalized SS coupons after exposure in the sterile and the *D. desulfuricans* inoculated SSMB medium for 3, 7, and 21 days, respectively. The linear portions of anodic and cathodic branches were extrapolated to their intersection to obtain the values of the Tafel slopes (b_a and b_c), corrosion potentials (E_{corr}), and corrosion current densities (i_{corr}) using procedures described previously (Yuan et al., 2007). The results are summarized in Table II. The corrosion potential, E_{corr} of the pristine coupons remains relatively constant with exposure time in the sterile SSMB medium, while it undergoes an active shift with exposure time in the *D. desulfuricans* inoculated SSMB medium, and decreases rapidly to about −500 mV after 7 days of exposure. The phenomenon is usually attributed to the anodic dissolution process in terms of the mixed potential theory (Huang et al., 2004). E_{corr} of the surface-functionalized coupons undergoes a noble shift, relative to those of the pristine SS coupons, in the *D. desulfuricans* inoculated medium (Table II). The ennoblement in E_{corr} is a common phenomenon for the polymer-coated coupons as compared to the bare metal coupons (Spinks et al., 2002). The corrosion current density, i_{corr}, of the pristine coupons remains small, even undergoes a slight decrease, in the sterile SSMB medium due to the passivity of surface film (including surface passivation arising from the conditioning layer of yeast extract), However, it increases steadily with exposure time in the *D. desulfuricans* inoculated SSMB medium, indicative of the enhancement of corrosion by *D. desulfuricans*. As for the surface-functionalized coupons, the corrosion current densities are significantly reduced. The magnitude of i_{corr} for the SS-*g*-QP(DMAEMA) and the SS-*g*-QP(DMAEMA)-Viologen coupons is lower by about 20- and 30-folds, respectively, as compared to that of the pristine SS coupon after 21 days of exposure in the *D. desulfuricans* inoculated medium, indicating that the surface-grafted polymer possess the desired capability against the synergistic effect of aggressive Cl^-, biogenic S^{2-} and bacterial cells of *D. desulfuricans*. The IE of the two surface-functionalized coupons are calculated on the basis of Equation 1 (Experimental Section and Table II). The IE values of the SS-*g*-QP(DMAEMA)-Viologen coupons are always larger than those of the SS-*g*-QP(DMAEMA) coupons, suggesting that the anticorrosion capability of the grafted polymer is substantially enhanced by the coupled viologen moieties.

Figure 10 shows the impedance spectra of the pristine and the surface-functionalized coupons after exposure in the sterile and the *D. desulfuricans* inoculated SSMB medium for 3, 7, and 21 days. The impedance spectra are usually analyzed by fitting with appropriate equivalent electrical circuits (EECs). The program EQUIVCRT by Boukamp was used to iteratively adjust the values of circuit elements to achieve the best match between the experimental and the fitted data (Boukamp, 1986). Three EECs were proposed to model the respective impedance spectra of the pristine and the surface-functionalized SS coupons (Fig. 11). ECC (a) is used to fit the impedance spectra of coupons with a compact surface film, ECC (b) is used to model the impedance spectra of coupons with porous and non-protective surface film, while ECC (c) has been widely used to estimate the barrier, protection and degradation of the polymer coatings (Mansfeld et al., 1986). In ECC (c), the pore resistance (R_{po})

Table II. Analysis of Tafel plots of the pristine and the surface-functionalized coupons after various exposure periods in the sterile and the D. desulfuricans inoculated SSMB medium.

Time (days)	Samples	b_a[a] (mV/dec)	b_c[b] (mV/dec)	$E_{corr.}$[c] (V)	$i_{corr.}$ (μA cm^{-2})	IE[d] (%)
3	Pristine (sterile)[e]	299	−367	−0.127	4.13	—
	Pristine (inoculated)[f]	203	−178	−0.350	11.35	—
	SS-*g*-QP(DMAEMA)	270	−280	−0.229	6.09	46.34
	SS-*g*-QP(DMAEMA)-Viologen	293	−285	−0.193	3.57	68.55
7	Pristine (sterile)	269	−360	−0.123	3.72	—
	Pristine (inoculated)	247	−183	−0.494	25.14	—
	SS-*g*-QP(DMAEMA)	325	−272	−0.225	6.48	74.22
	SS-*g*-QP(DMAEMA)-Viologen	282	−277	−0.196	4.58	81.78
21	Pristine (sterile)	264	−318	−0.13	3.84	—
	Pristine (inoculated)	488	−181	−0.536	129.10	—
	SS-*g*-QP(DMAEMA)	268	−292	−0.226	6.64	94.78
	SS-*g*-QP(DMAEMA)-Viologen	278	−286	−0.183	4.94	96.17

[a]b_a is the Tafel slope of the anodic polarization curve.
[b]b_c is the Tafel slope of the cathodic polarization curve.
[c]E_{corr} refers to the potential, where the current reaches zero under polarization.
[d]IE denotes inhibition efficiency.
[e]Pristine (sterile) refers to the pristine coupons exposed to the sterile SSMB medium.
[f]Pristine (inoculated) refers to the pristine coupons exposed to the *D. desulfuricans* inoculated SSMB medium.

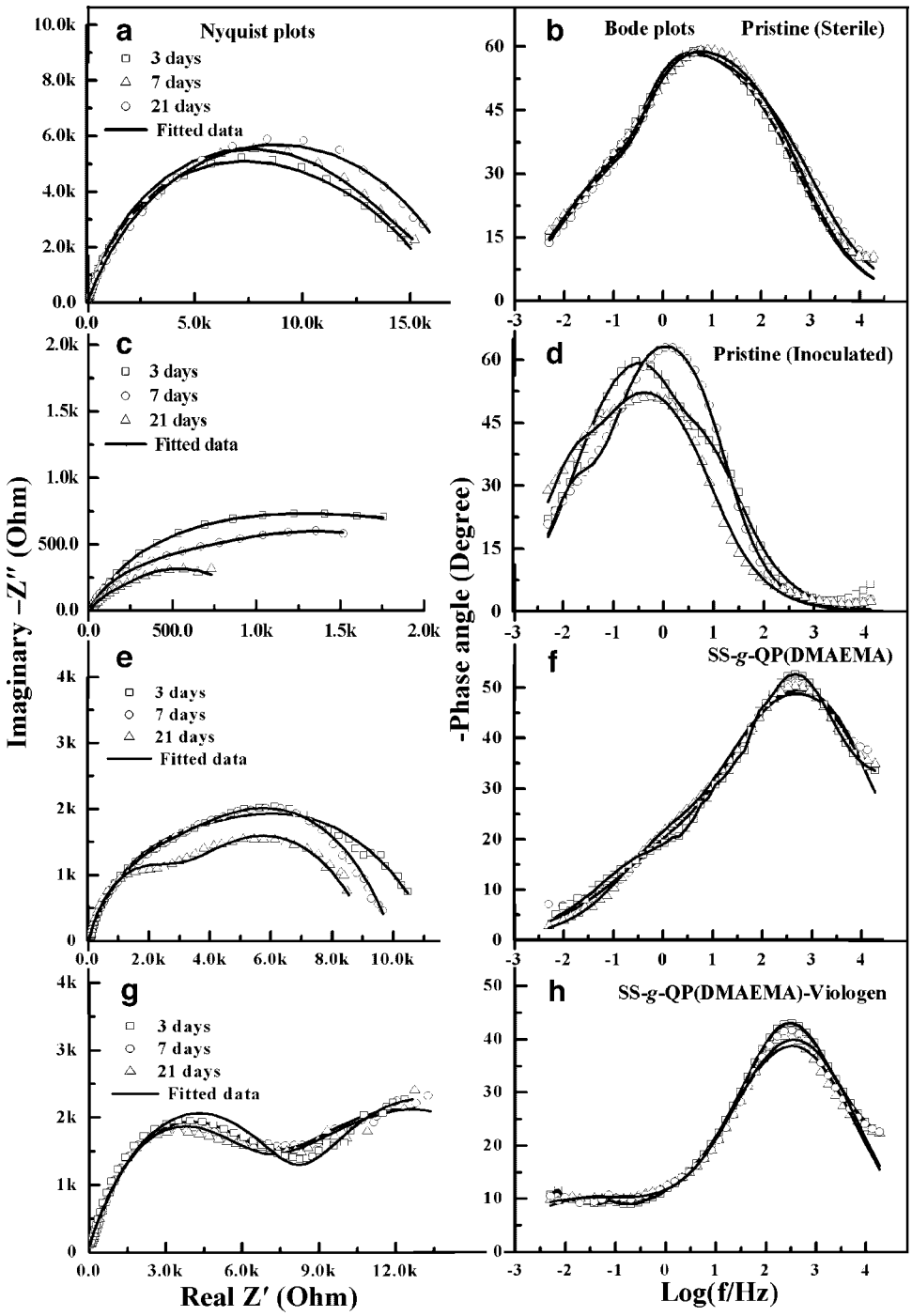

Figure 10. Impedance spectra of (**a**,**b**) the pristine coupons after exposure to the sterile SSMB medium for 3, 7, and 21 days, and (**c**,**d**) the pristine, (**e**,**f**) the SS-*g*-QP(DMAEMA), and (**g**,**h**) the SS-*g*-QP(DMAEMA)-Viologen coupons after 3, 7, and 21 days of exposure in the *D. desulfuricans* inoculated SSMB medium. The solid lines show the fitted results based on the corresponding equivalent circuits.

represents the extent of ionic conduction through a polymer in an electrolytic environment, and is commonly used as a criterion for assessing the extent of corrosion protection derived from the organic coatings, while the constant phase elements (CPE) of coating, Q_c, is used to substitute coating capacitance, C_c, by taking into account of the phenomena related to the heterogeneous surface and diffusion process (Mansfeld et al., 1986; Yuan et al., 2007).

The fitted parameters of the impedance spectra are summarized in Table III. For the pristine SS coupon in the sterile medium, the charge transfer resistance, R_{ct}, and the resistance of surface film, R_f, undergo a slight increase

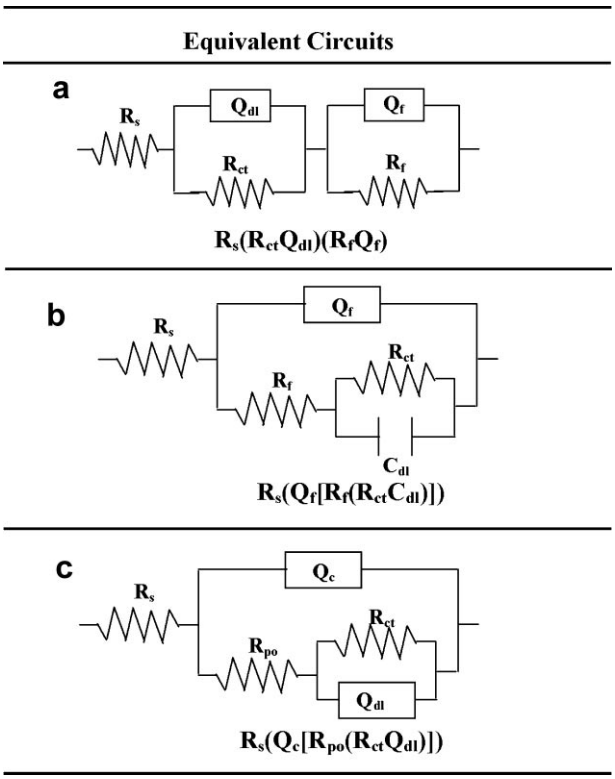

Figure 11. Equivalent circuits used for fitting the impedance spectra of (**a**) the pristine (in the sterile medium), (**b**) the pristine (in the inoculated medium), and (**c**) the surface-functionalized coupons.

with exposure time, attributable to the passivation of the conditioning layer of yeast extract. R_{ct} of the pristine coupons in the *D. desulfuricans* inoculated medium decreases gradually with exposure time, indicative of the enhancement of corrosion by *D. desulfuricans*. The resistance of surface film, R_f, increases initially with exposure time due to the formation of porous iron sulfide layer in the *D. desulfuricans* inoculated medium, and then decreases with the exposure time as a result of the initiation of localized corrosion beneath the corrosion deposits. In the case of the surface-functionalized coupons, R_{ct} values of the two surface-functionalized coupons are significantly larger than that of the pristine SS coupon throughout the exposure periods in the *D. desulfuricans* inoculated medium, indicative of the decrease in corrosion rate of the SS coupons under the protection of grafted polymer layer. On the other hand, the pore resistance, R_{po}, of the SS-*g*-QP(DMAEMA)-Viologen coupon is markedly larger than that of the corresponding SS-*g*-QP(DMAEMA) coupon throughout the exposure periods, indicative of the substantial increase in barrier property of the grafted polymer-viologen coating against the penetration of aggressive ions and water. The capacitance (Q_c) of coating as a function of exposure time in an electrolyte solution provides information on stability of the coating and the extent of water uptake (Mansfeld et al., 1986). Q_c of the SS-*g*-QP(DMAEMA) coupons increases gradually with exposure time, indicative of the uptake of the electrolyte and water by the grafted polymer coatings, and thus the decrease in protective capability of the grafted polymer coating on the SS-*g*-QP(DMAEMA) surface. Q_c of the SS-*g*-QP(DMAEMA)-Viologen coupon remains constant with exposure time, indicative of improved stability of the grafted polymer coating with the incorporated viologen moieties. It is worthy to note that the passivating silane layer beneath the grafted polymer coatings also plays a role in rendering anticorrosion properties to the substrate surface, since the self-assembled silane monolayer has been widely reported to protect metallic substrates from corrosion damages (Zucchi et al., 2004).

Table III. Fitting parameters of the EIS spectra of the pristine and the surface-functionalized coupons after various exposure periods in the sterile and the D. desulfuricans inoculated SSMB medium.

		Parameters												
					Q_{dl}			Q_f			Q_c			
Samples	Time (days)	R_s (Ω)	R_{ct} (kΩ)	C_{dl} (μF)	$Y_0 \times 10^{-4}$ (Ω^{-1} s^n)	n_0	R_f (kΩ)	$Y_1 \times 10^{-5}$ (Ω^{-1} s^n)	n_1	R_{po} (kΩ)	$Y_2 \times 10^{-4}$ (Ω^{-1} s^n)	n_2	$\sum\chi^2 \times 10^{-3}$
Pristine (sterile)[a]	3	12.95	11.68	—	1.76	0.69	4.65	26.32	0.74	—	—	—	1.20
Pristine (inoculated)[b]		13.22	2.01	0.48	—	—	0.25	20.98	0.72	—	—	—	0.49
SS-*g*-QP(DMAEMA)[c]		24.40	7.78	—	0.90	0.58	—	—	—	4.20	1.38	0.64	3.49
SS-*g*-QP(DMAEMA)-Viologen[c]		27.41	11.92	—	2.92	0.48	—	—	—	6.89	0.68	0.61	4.93
Pristine (sterile)	7	12.31	12.31	—	1.33	0.55	5.56	53.75	0.84	—	—	—	2.15
Pristine (inoculated)		11.76	0.84	15.65	—	—	1.00	18.42	0.83	—	—	—	2.18
SS-*g*-QP(DMAEMA)		27.31	7.27	—	1.09	0.46	—	—	—	4.10	1.21	0.64	5.99
SS-*g*-QP(DMAEMA)-Viologen		24.38	12.22	—	2.81	0.36	—	—	—	6.27	0.64	0.62	4.52
Pristine (sterile)	21	13.15	11.75	—	1.83	0.68	5.14	46.76	0.83	—	—	—	1.16
Pristine (inoculated)		12.27	0.41	39.64	—	—	0.55	4.80	0.73	—	—	—	3.31
SS-*g*-QP(DMAEMA)		26.93	6.09	—	1.59	0.55	—	—	—	3.15	0.78	0.71	8.39
SS-*g*-QP(DMAEMA)-Viologen		22.05	11.49	—	3.48	0.38	—	—	—	6.37	0.62	0.58	3.21

[a]EIS data of the pristine coupons in the sterile SSMB medium are fitted with equivalent circuit (a) of Figure 11.
[b]EIS data of the pristine coupons in the *D. desulfuricans* inoculated SSMB medium are fitted with equivalent circuit (b) of Figure 11.
[c]EIS data of the surface-functionalized coupons in the inoculated SSMB medium are fitted with equivalent circuit (c) of Figure 11.

Stability of the Functionalized Substrate Surface

As cracks and crevice in organic coatings have been widely recognized to produce localized dissolution which can be even more serious than that produced by biofilms, it is appropriate to emphasize the stability and durability of the grafted polymeric coatings. For the SS-*g*-QP(DMAEMA) and the SS-*g*-QP(DMAEMA)-viologen coupons exposed to the *D. desulfuricans* inoculated SSMB medium for 21 days, the XPS results suggested that the composition of the functionalized surfaces remained almost unchanged, indicative of the stability and reliability of the covalently tethered QP(DMAEMA) and QP(DMAEMA)-viologen brushes on the substrate surfaces. Moreover, silanization of metallic surfaces to reduce their reactivity is a well-established process. The silane layers coupled on the substrate surface via robust Si–O bond have been found to be stable in acidic solutions (Zucchi et al., 2004). Moreover, the well-defined polymeric brushes grafted on various substrate surfaces, including glass, fibre, paper, silicon wafer, and SS, via surface-initiated ATRP have been shown to be stable under harsh environments (Fan et al., 2006; Lee et al., 2004; Xu et al., 2006). Further studies focusing on long-term performance of polymer brushes in biocorrosion protection of the surface-functionalized SS coupons are in progress.

Conclusions

A novel approach to combat biocorrosion by grafting of well-structured polymer coatings (brushes) from the SS surfaces, via surface-initiated ATRP, was demonstrated. The process involved: (i) covalent immobilization of an alkyl halide ATRP initiator monolayer on the hydroxylated stainless steel (SS-OH) surface via the action of a trichlorosilane coupling agent, (ii) functionalizing the silane-coupled substrate surface by grafted P(DMAEMA) brushes from surface-initiated ATRP of DMAEMA, (iii) quaternization of the P(DMAEMA) brushes via N-alkylation or coupling of viologen to introduce the quaternary ammonium moieties. The viologen-quaternized SS-*g*-QP(DMAEMA) surface with a substantially higher N^+ concentration on the surface, exhibits enhanced antibacterial properties over those of the benzyl halide-quaternized SS-*g*-QP(DMAEMA) surface, and can thus inhibit bacterial adhesion and growth more effectively. Electrochemical analysis results revealed that the grafted polymer coatings were effective in protecting the substrate from biocorrosion by *D. desulfuricans*, with the anticorrosion capability markedly enhanced by the surface-coupled viologen layers. In comparison, the pristine SS was found to be vulnerable to biocorrosion by *D. desulfuricans*.

The authors would like to thank the National University of Singapore for the financial support of this study under the FRC Research Grant R-279-000-236-112.

References

Akid R, Wang HM, Smith TJ, Greenfield D, Earthman JC. 2008. Biological functionalization of a sol-gel coating for the mitigation of microbial-induced corrosion. Adv Funct Mater 18:203–211.

Al-Darbi MM, Muntasser ZM, Tango M, Islam MR. 2002. Control of microbial corrosion using coatings and natural additives. Energ Source 2002. 24:1009.

Antony PJ, Chongdar S, Kumar P, Raman R. 2007. Corrosion of 2205 duplex stainless steel in chloride medium containing sulfate-reducing bacteria. Electrochim Acta 52:3985–3994.

Beech IB, Sunner J. 2004. Biocorrosion: Towards understanding interactions between biofilms and metals. Curr Opin Biotech 15:181–186.

Boukamp BA. 1986. A nonlinear least-square fit procedure for analysis of immittance data of electrochemical systems. Solid State Ionics 20:31–44.

Braunecker WA, Matyjaszewski K. 2007. Controlled/living radical polymerization: Features, developments, and perspectives. Prog Polym Sci 32:93–146.

Cetin D, Bilgic S, Dönmez G. 2007. Biocorrosion of low alloy steel by *Desulfotomaculmum sp* and effect of biocides on corrosion control. ISIJ Int 47:1023–1028.

de Mele MFL, de Saravia SGG, Videla HA. 1995. An overview on biofilms and calcareous deposits interactions on cathodically protected steel surface. In: Angell P, Boronstein SW, editors. Proceedings of the 1995 international conference on microbially influenced corrosion. New Orleans: NACE. p. 501–508.

Fan XW, Lin LJ, Dalsin JL, Messersmith PB. 2005. Biomimetic anchor for surface-initiated polymerization from metal substrates. J Am Chem Soc 127:15843–15847.

Fan XW, Lin LJ, Massersmith PB. 2006. Cell fouling resistance of polymer brushes grafted from Ti substrates by surface-initiated polymerization: effect of ethylene glycol side chain length. Biomacromolecules 7:2443–2448.

Flemming HC. 1996. Biofouling and microbially influenced corrosion (MIC)—An economical and technical overview. In: Heitz E, Flemming HC, Sand W, editors. Microbially influenced corrosion of materials: Scientific and engineering aspects. Berlin: Springer Verlag. p 5–14.

Fu JH, Ji J, Yuan WH, Shen JC. 2005. Construction of antiadhesive and antibacterial multilayer films via layer-by-layer assembly of heparin and chitosan. Biomateirals 26:6684–6692.

Guezennec JG. 1994. Cathodic protection and microbially induced corrosion. Int Biodeter Biodegr 34:275–288.

Hamilton WA. 1985. Sulfate-reducing bacteria and anaerobic corrosion. Annu Rev Microbiol 39:195–217.

Hu FX, Neoh KG, Kang ET. 2005. Antibacterial and antifungal efficacy of surface functionalized polymer beads in repeated applications. Biotechnol Bioeng 89:474–484.

Hu FX, Neoh KG, Cen L, Kang ET. 2006. Cellular response to magnetic nanoparticles "PEGylated" via surface-initiated atom transfter radical polymerization. Biomacromolecules 7:809–816.

Huang GT, Chan KY, Fang HHP. 2004. Microbiologically induced corrosion of 70Cu-30Ni alloy in anaerobic seawater. J Electrochem Soc 151:B434–B439.

Iverson WP. 1966. Direct evidence for the cathodic depolarization theory of bacterial corrosion. Science 151:986–988.

Jack RF, Ringelberg DB, White DC. 1992. Differential corrosion rates of carbon steel by combinations of *Bacillus sp*, *Hafnia-alvei* and *Desulfovibrio gigas* established by phospholipid analysis of electrode biofilm. Corros Sci 33:1843–1853.

Jelic-Mrcelic G, Sliskovic M, Antolic B. 2006. Biofouling communities on test panels coated with TBT and TBT-free copper based antifouling paints. Biofouling 22:293–302.

Lee SB, Koepsel RR, Morley SW, Matyjaszewski K, Sun YJ, Russell AJ. 2004. Permanent, nonleaching antibacterial surfaces. 1. Synthesis by atom transfer radical polymerization. Biomacromolecules 5:877–882.

Lin J, Qiu SY, Lewis K, Klibanov AM. 2003. Mechanism of bactericidal and fungicidal activities of textiles covalently modified with alkylated polyethylenimine. Biotechnol Bioeng 83:168–172.
Little BJ, Wagner PA. 1993. The interrelationship between marine biofouling and cathodic protection. Mater Performance 32:16–20.
Little BJ, Ray RI, Pope RK. 2000. Relation between corrosion and the biological sulfur cycle: A review. Corrosion 56:433–443.
Liu Y, Wang L, Pan CY. 1999. Synthesis of block copoly(styrene-*b*-*p*-nitrophenol methacrylate) and its derivatives by atom transfer radical polymerization. Macromolecules 32:8301–8305.
Mansfeld F, Jeanjaquet SL, Kendig MW. 1986. An electrochemcial impedance spectroscopy study of reactions at the metal-coating interface. Corros Sci 28:735–742.
Martin HJ, Schulz KH, Bumgardner JD, Walters KB. 2007. XPS study on the use of 3-aminopropyltriethoxysilane to bond chitosan to a titanium surface. Langmuir 23:6645–6651.
Milović NM, Wang J, Lewis K, Klibanov AM. 2005. Immobilized *N*-alkylated polyethylenimine avidly kills bacteria by rupturing cell membranes with no resistance developed. Biotechnol Bioeng 90:715–722.
Miyanaga K, Terashi R, Kawai H, Unno H, Tanji Y. 2007. Biocidal effect of cathodic protection on bacterial viability in biofilm attached to carbon steel. Biotechnol Bioeng 97:850–857.
Mohanan S, Maruthamuthu S, Kalaiselvi N, Palaniappan R, Venkatachari G, Palaniswamy N, Raghavan M. 2005. Role of quaternary ammonium compounds and ATMP on biocidal effect and corrosion inhibition of mild steel and copper. Corros Rev 23:425–444.
Monk PMS. 1998. The viologens: Physicochemical properties synthesis and applications of the salts of 4,4′-bipyridine. New York: John Wiley & Sons. p 32–54.
Moreno DA, de Mele MFL, Ibars JR, Videla HA. 1991. Influence of microstructure on the electrochemical behavior of type-410 stainless steel in chloride media with inorganic and biogenic sulfide. Corrosion 47:2–9.
Muthukumar N, Maruthamuthu S, Mohanan S, Palaniswamy N. 2007. Influence of an oil soluble inhibitor on microbiologically influenced corrosion in a diesel transporting pipeline. Biofouling 23:395–404.
Popova A, Christov M, Vasilev A. 2007. Inhibitive properties of quaternary ammonium bromide of N-containing heterocycles on acid mild steel corrosion. Part II: EIS results. Corros Sci 49:3290–3302.
Shibata T, Okamoto G. 1978. Passivity and breakdown of passivity of stainless steel. In: Frankenthal RP, Kruger J, editors. Passivity of metals. New York: Electrochem Soc Inc. p 521–545.
Spinks GM, Dominis AJ, Wallace GG, Tallman DE. 2002. Electroactive conducting polymers for corrosion control-Part 2 ferrous metals. J Solid State Electr 6:85–100.
Sreekumari KR, Sato Y, Kikuchi Y. 2005. Antibacterial metals: A viable solution for bacterial attachment and microbiologically influenced corrosion. Mater Trans 46:1636–1645.
Tait WS. 1978. Comparison of potentiodynamically determined pitting rates with actual pitting rates for mild steel and admiralty brass in oxygen bearing water. Corrosion 34:214–218.
Tait WS. 1979. Effect of physical parameters on the pitting corrosion of mild steel in low total dissolved solids, oxygen bearing waters: A nonpassivating metal-environment system. Corrosion 35:296–300.
Telegdi J, Rigó T, Beczner J, Kálmán E. 2005. Influence of Langmuir-Blodgett nanolayers on microbial adhesion. Surf Eng 21:107–112.
Tiller JC, Liao CJ, Lewis K, Klbanov AM. 2001. Designing surfaces that kill bacteria on contact. Proc Natl Acad Sci 11:5981–5985.
Tiller JC, Lee SB, Lewis K, Klibanov AM. 2002. Polymer surfaces derivatized with poly(vinly-*N*-hexylpyridinium) kill airborne and waterborne bacteria. Biotechnol Bioeng 79:465–471.
Tributsch H, Rojas-Chapana JA, Bätels CC, Ennaoui A, Hofmann W. 1998. Role of transient iron sulfide films in microbial corrosion of steel. Corrosion 54:216–227.
Videla HA. 2002. Prevention and control of biocorrosion. Int Biodeter Biodegr 49:259–270.
Wagner CD, Moulder JF, Davis JE, Riggs WM. 1992. Handbook of X-ray photoelectron spectroscopy. Minnesota: Perkin-Elmer Corp.
Wang JS, Matyjaszewski K. 1995. Controlled ''living'' radical polymerization. Atom transfer radical polymerization in the presence of transition-metal complexes. J Am Chem Soc 117:5614–5615.
Xu FJ, Yuan SJ, Pehkonen SO, Kang ET, Neoh KG. 2006. Antimicrobial surfaces of viologen-quaternized poly(2-dimethylamino)ethyl methacrylate-Si(100) hybrids from surface-initiated atom transfter radical polymerization. Nanobiotechnology 2:123–134.
Yebra DM, Kiil S, Dam-Johansen K. 2004. Effects of marine microbial biofilms on the biocide release rate from antifouling paints—A model-based analysis. Prog Org Coat 50:75–104.
Yuan SJ, Xu FJ, Kang ET, Pehkonen SO. 2007. Modification of surface-oxidized copper alloy by coupling of viologens for inhibiting microbiologically influenced corrosion. J Electrochem Soc 154:C645–C657.
Yuan SJ, Xu FJ, Pehkonen SO, Ting YP, Neoh KG, Kang ET. 2008. Biocorrosion behavior of titanium oxide/butoxide-coated stainless steel. J Electrochem Soc 155:C196–C210.
Zhao BZ, Neoh KG, Kang ET. 2002. Environmental stability of electrically conductive viologen-polyaniline systems. J Appl Polym Sci 86:2099–2107.
Zucchi F, Grassi V, Frignani A, Trabanelli G. 2004. Inhibition of copper corrosion by silane coatings. Corros Sci 46:2853–2865.